J. Fluid Mech. (1990), *vol.* 214, *pp.* 229–250
Printed in Great Britain

Non-uniqueness and bifurcation in annular and planar channel flows

By M. S. BORGAS[1] AND T. J. PEDLEY[2]

[1] CSIRO, Division of Atmospheric Research, Private Bag No. 1, Mordialloc, Victoria 3195, Australia

[2] Department of Applied Mathematical Studies, The University, Leeds LS2 9JT, UK

(Received 19 June 1989)

High-Reynolds-number steady flow in an annular pipe which encounters a shallow axisymmetric expansion or indentation in the walls is studied using interactive boundary-layer theory. The flow upstream of the indentation ($x < 0$) is fully developed; the ratio of the shear rate on the outer wall to that on the inner wall is denoted by ρ ($0 < \rho \leqslant 1$); similarity solutions are found for the case where the wall perturbations are proportional to $x^{\frac{1}{3}}$. The solution is unique in a constriction, when the pressure gradient (represented by a parameter b) is favourable ($b < 0$). In an expansion, however, with an adverse pressure gradient, three different solutions are found if b exceeds a critical value b_c. When $\rho \neq 1$, one of these solutions, representing a flow that is attached on the inner wall and separated (i.e. has negative wall shear) on the outer, is a continuation of the unique doubly attached flow at small b. The other two, one separated on the inner and not the outer wall and the other separated on both walls, arise from a saddle-node bifurcation at $b = b_c$. The doubly separated flow is never stable, as observed in diffusers. In the case of a planar channel ($\rho = 1$) symmetry is restored, and the non-uniqueness arises through a supercritical pitchfork bifurcation. This agrees with previous computations on channel flow, but not with Jeffery–Hamel flow, for which the bifurcation is subcritical.

1. Introduction

It is well known that steady flow in a diffuser, that is a pipe or channel whose cross-sectional area increases gradually with distance, is usually non-unique. Even when the geometry is symmetric, so that a symmetric solution to the equation of motion must exist, the flow is normally asymmetric, clinging to one wall or another (figure 1; see Reneau, Johnston & Kline 1967; Ward-Smith 1980); only when the expansion is sharp is the symmetric 'jet flow' observed. Sobey & Drazin (1986) have studied experimentally and numerically the flow in a two-dimensional channel which consists of a long straight segment (of length Lh and width Dh) with a smooth symmetric constriction to width h and re-expansion at each end (the numerical results were obtained with periodic boundary conditions); typically L was 80 and D (> 1) took values up to 3. They showed that the symmetric flow, which does involve separation and negative fluid velocities, as depicted in fig. 1(*a*), is stable at sufficiently low values of the Reynolds number $R = Q/\nu$ (where Q is the volume flow rate per unit depth of the channel and ν is the fluid kinematic viscosity; this definition of R is a factor of 2 greater than in Sobey and Drazin's notation), but that it experiences a supercritical pitchfork bifurcation (or a series of such bifurcations) for R between about 12 and about 40 (when $D = 3$), above which one of the two equivalent

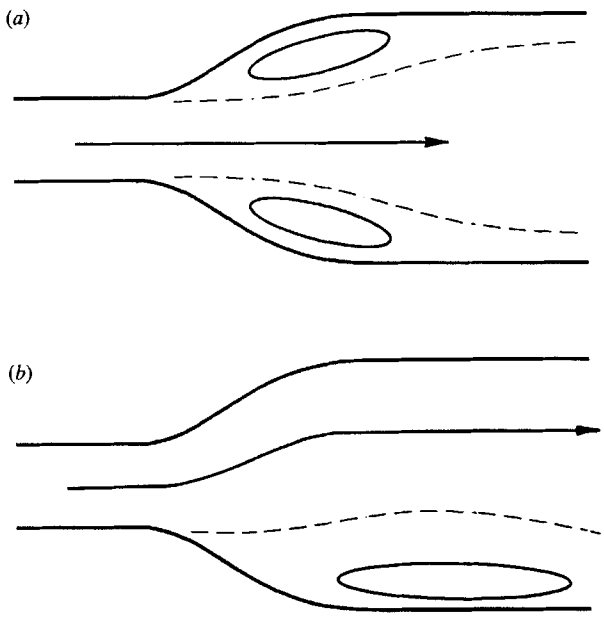

FIGURE 1. Sketches of symmetric and asymmetric flow in a symmetric expansion; the symmetric flow is unstable and not observed except at very small Reynolds number.

asymmetric flows is stable. Sobey (1985) made similar observations for flow in a channel consisting of two long segments (widths h and $3h$) with a smooth symmetric expansion between them. Sobey & Drazin went on to show that the bifurcation structure of the space of possible flows in this geometry becomes quite intricate at larger values of R.

These authors, together with Banks, Drazin & Zaturska (1988), sought to model the bifurcation structure of non-uniform channel flow by examining the simpler geometry of Jeffery–Hamel flow between plane walls inclined at an angle 2α. Building on the pioneering work of Fraenkel (1962, 1963), they showed (among other things) that, at fixed but non-zero x, the first bifurcation to occur as R is increased is a *sub*critical pitchfork, at $R = R_c(\alpha)$, where $R_c \sim 9.42/\alpha$ as $\alpha \to 0$, and above that value a stable asymmetric flow cannot be found. Thus Jeffery–Hamel flow is shown not to be a very good model for the experimental situation, and examining bifurcations in other simple channel flows could be of considerable interest, to see if they are more relevant to the experiments, or are better modelled by Jeffery–Hamel flow, or indeed exhibit yet another, different type of initial bifurcation.

A feature of Jeffery–Hamel flow is that no bifurcations are found if the boundary-layer approximation is made at the start, i.e. if $\alpha \to 0$ with αR held constant, and then αR is increased. In this paper we examine a class of channel flows which are governed by the boundary-layer equations, and we find non-uniqueness and bifurcation in them. The analogous external flow is the Falkner–Skan boundary layer undergoing a small adverse pressure gradient (see Banks & Drazin 1973). (Smith 1984, has pointed out the presence of non-uniqueness in unbounded flows governed by the boundary-layer equations with *zero* external pressure gradient (wakes and external boundary layers), the non-standard flows involving large regions of reversed flow. He speculates, however, that a downstream obstacle of some sort will be required to

generate the flows in question, since experimental and numerical evidence suggests that the standard solutions exist and are stable until instability sets in.)

The flow to be considered in this paper is a generalization of one that was also previously examined by Smith (1976*a*): high-Reynolds-number flow in a parallel-sided channel which encounters a shallow indentation or expansion in one or both walls. The scalings are such that the oncoming Poiseuille flow is merely displaced and viscosity has no influence except in thin boundary layers on the walls. The generalization here is to treat annular as well as planar channels; the application we had in mind was to understand the effect of inserting a catheter with a balloon of variable diameter on it into an artery (such a device is used in the aorta to give assistance to a weak heart, especially during surgery); annular diffusers are used in engineering contexts too (Ward-Smith 1980). Mathematically the results are as easy to compute and to interpret in the annular case, the planar case being but one limit. The detailed calculations are made using similarity solutions to the equations for a class of expansion shapes in which the height of the perturbation is proportional to $x^{\frac{1}{3}}$, where x is the distance downstream from the start of the expansion.

The conclusion is that the flow is non-unique in channels with a sufficiently adverse pressure gradient (b, say). For planar channels there is a *supercritical* pitchfork bifurcation at a critical value of b, say b_c. For $b < b_c$ the flow is attached on both walls, whilst the two (presumably) stable flows for $b > b_c$ are separated on one wall and attached on the other. The unstable symmetric flow for $b > b_c$ is separated on both walls. For an annular geometry this symmetry is broken, and the bifurcation diagram splits into two branches, only one of which connects to the unique small-b solution. The doubly separated flow is still unstable, however.

The problem is formulated in §2 and solved in §3; §3.1 contains the small-$|b|$ solution, §3.2 contains an inviscid large-$|b|$ solution which may not represent a realizable flow but raises the possibility of non-uniqueness, while §3.3 contains the similarity solutions. The bifurcation structure is discussed in §4, and §5 provides further discussion, mainly on the implications for more general channel flows and their computation.

2. Formulation

The unperturbed annular pipe is taken to have radii a_0, $a_0\beta$ ($\beta > 1$) and the oncoming parallel flow has velocity profile $U_0^* U_0(r)$, where $a_0 r$ is the radial coordinate,

$$U_0(r) = \frac{-(r^2-1)\log\beta + (\beta^2-1)\log r}{\beta^2 - 1 - 2\log\beta} \tag{2.1}$$

and the velocity scale U_0^* has been chosen to that $U_0'(1) = 1$. The dimensionless shear rate at the outer wall is

$$\rho = -U_0'(\beta) = \frac{2\beta^2\log\beta + 1 - \beta^2}{\beta(\beta^2-1) - 2\beta\log\beta} < 1. \tag{2.2}$$

As $\beta \to \infty$, $\rho \sim 2\log\beta/\beta$; in the planar limit, both β and ρ become 1.

The walls are taken to be unperturbed for $x < 0$, where the longitudinal coordinate is taken to be $a_0\lambda x$, $\lambda(\gg 1)$ being a scaling to be specified. For $x > 0$ we take the walls to be at

$$r = 1 + \epsilon F(x), \quad r = \beta - \epsilon\tilde{F}(x), \tag{2.3}$$

where $\epsilon(\ll 1)$ is the amplitude parameter. Following Smith (1976*a*) we take

$$\epsilon = R^{-\frac{1}{2}}\alpha^{-\frac{1}{2}}, \quad \lambda = R^{-\frac{1}{2}}\alpha^{-\frac{3}{2}}, \tag{2.4}$$

where $\alpha(=\epsilon/\lambda)$ is a scale for the slope of the perturbed walls. This must lie in the range

$$R^{-1} \ll \alpha \ll R^{-\frac{3}{7}}$$

so that viscous forces are not important over the whole cross-section ($R^{-1} \ll \alpha$) and the cross-stream pressure gradient induced by the disturbance is negligible. The viscous boundary layers have dimensionless thickness ϵ.

The Navier–Stokes and continuity equations are expressed in terms of cylindrical polar coordinates $(a_0\lambda x, a_0 r, \theta)$, with corresponding velocity components $U_0^*(u, \lambda^{-1}v, 0)$ and pressure $-\mu U_0^* k\lambda x/a_0 + \rho U_0^{*2} p$ (where k is a numerical constant). In dimensionless form the equations are

$$(ru)_x + (rv)_r = 0, \tag{2.5}$$

$$uu_x + uv_r = -p_x + \frac{\lambda}{R}\left(u_{rr} + \frac{1}{r}u_r + \lambda^{-2}u_{xx}\right), \tag{2.6}$$

$$uv_x + vv_r = -\lambda^2 p_r + \frac{\lambda}{R}\left(v_{rr} + \frac{1}{r}v_r - \frac{v}{r^2} + \lambda^{-2}v_{xx}\right). \tag{2.7}$$

In the core, away from the walls, viscosity is negligible and when the velocity field is expanded in powers of ϵ, the first perturbation is found to be a pure radial displacement of the streamlines with no cross-stream pressure gradient:

$$\left.\begin{aligned} u &= U_0(r) + \epsilon U_1(x, r) + \ldots \\ v &= \epsilon V_1(x, r) + \ldots, \quad p = \epsilon^2 P(x) + \ldots, \end{aligned}\right\} \tag{2.8}$$

where

$$U_1 = A(x)\, U_0'(r)/r, \quad V_1 = -A'(x)\, U_0(r)/r. \tag{2.9}$$

The displacement function $A(x)$ and pressure perturbation function $P(x)$ are as yet arbitrary.

At a dimensionless distance of ϵ from the walls both U_0 and ϵU_1 are of the same order of magnitude and, since $\epsilon = (\lambda/R)^{\frac{1}{3}}$, the viscous terms in (2.6) become as important as the inertia terms. We rescale the variables accordingly in the two boundary layers, and make the Prandtl transformation. Thus in the layer near $r = 1$ we write

$$r = 1 + \epsilon[F(x) + Y], \quad p = \epsilon^2 P(x),$$

$$u = \epsilon U(x, Y), \quad v = \epsilon^2[V(x, Y) + U(x, Y)\, F'(x)],$$

giving the following boundary-layer problem:

$$UU_x + VU_y = -P'(x) + U_{yy}, \quad U_x + V_y = 0, \tag{2.10a}$$

$$U = V = 0 \quad \text{on} \quad Y = 0, \tag{2.10b}$$

$$U \sim Y + F(x) + A(x) \quad \text{as} \quad Y \to \infty. \tag{2.10c}$$

In the layer near $r = \beta$ we also write

$$r = \beta - \epsilon[\tilde{F}(x) + \tilde{Y}], \quad p = \epsilon^2 P(x),$$

$$u = \epsilon\tilde{U}(x, \tilde{Y}), \quad v = -\epsilon^2[\tilde{V}(x, \tilde{Y}) + \tilde{U}(x, \tilde{Y})\, \tilde{F}'(x)],$$

which lead to the same equations and wall boundary conditions, (2.10a, b), for $\tilde{U}$, $\tilde{V}$ as for U, V, but the outer boundary condition is different:

$$U \sim \rho\left(\tilde{Y} + \tilde{F} - \frac{A}{\beta}\right) \quad \text{as} \quad \tilde{Y} \to \infty. \tag{2.11}$$

Smith (1976*a*) noticed that, in the planar case $\rho = \beta = 1$, the two boundary-layer problems are identical, since the outer boundary condition could be written $U_y \to 1$ as $Y \to \infty$ or $\tilde{U}_{\tilde{y}} \to 1$ as $\tilde{Y} \to \infty$. Assuming a unique solution, he could therefore deduce that $F + A \equiv \tilde{F} - A$, and hence that

$$A = \tfrac{1}{2}(F - \tilde{F}). \tag{2.12}$$

The symmetry is broken when $\rho \neq 1$ so, even on the assumption of a unique solution, we cannot make a corresponding deduction without solving the boundary-layer problems first.

3. Solutions

3.1. *Linearized problem*

In the small-amplitude case the solution to the boundary-layer problems is unique, and we outline it only briefly since it directly follows that of Smith (1976*a*). We introduce a small parameter h, and set

$$A = ha(x), \quad F = hf(x), \quad \tilde{F} = h\tilde{f}(x), \quad P = hp(x),$$

$$U = y + h\bar{u}(x, Y), \quad V = h\bar{v}(x, Y), \quad \tilde{U} = \rho\tilde{Y} + h\tilde{u}(x, \tilde{Y}), \quad \tilde{V} = h\tilde{v}(x, \tilde{Y}).$$

The continuity equation and the wall boundary conditions are the same as in the nonlinear case (2.10*a*, *b*); the linearized momentum equations (2.10*a*) and outer boundary conditions (2.10*c*), (2.11) become

$$Y\bar{u}_x + \bar{v} = -p'(x) + \bar{u}_{yy}, \quad \rho\tilde{Y}\tilde{u}_x + \rho\tilde{v} = -p'(x) + \tilde{u}_{\tilde{y}\tilde{y}} \tag{3.1}$$

and

$$\bar{u} \to f + a \quad \text{as} \quad Y \to \infty, \quad \tilde{u} \to \rho(\tilde{f} - a/\beta) \quad \text{as} \quad \tilde{Y} \to \infty. \tag{3.2}$$

The problems are solved using Fourier transforms in x, with the notation

$$\hat{p}(k) = \int_{-\infty}^{\infty} p(x)\, \mathrm{e}^{-\mathrm{i}kx}\, \mathrm{d}x,$$

and it is seen that the transforms of the shear-rate perturbations, $\hat{\tau} = \hat{\bar{u}}_y$ and $\hat{\tilde{\tau}} = \hat{\tilde{u}}_{\tilde{y}}$, satisfy Airy's equation. The coefficients of the relevant Airy functions are expressed in terms of $\hat{p}$ by evaluating the transforms of (3.1) at $Y, \tilde{Y} = 0$, and two equations for $\hat{p}$ and $\hat{a}$ are then obtained from (3.2). The results are

$$\left.\begin{aligned} \hat{p} &= 3\,\mathrm{Ai}'(0)\,(\mathrm{i}k)^{-\frac{1}{3}} \frac{(\beta\hat{\tilde{f}} + \hat{f})}{1 + \beta/\rho^{\frac{5}{3}}}, \\ \hat{a} &= \frac{\rho^{\frac{5}{3}}\hat{\tilde{f}} - \hat{f}}{1 + \rho^{\frac{5}{3}}/\beta}, \end{aligned}\right\} \tag{3.3}$$

from the second of which we can deduce immediately how the displacement of the core flow depends on the wall shapes:

$$a(x) = \frac{\rho^{\frac{5}{3}}\tilde{f}(x) - f(x)}{1 + \rho^{\frac{5}{3}}/\beta}. \tag{3.4}$$

This formula can indeed be seen to reduce to (2.12) in the planar case $\rho = \beta = 1$.

Inversion of (3.3) and the corresponding transform of the wall shear perturbations $\tau_0, \tilde{\tau}_0$ is straightforward and yields no surprises, the results being qualitatively similar to those of Smith (1976*a*). For example, if

$$f(x) = x\,\mathrm{e}^{-x} H(x), \quad \tilde{f}(x) = 0$$

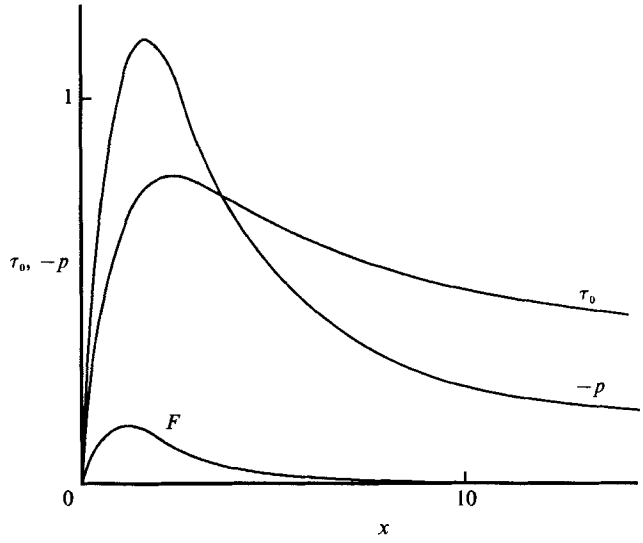

FIGURE 2. Normalized pressure and shear rate perturbations, as functions of x, calculated from linear theory for an indentation whose shape is given by $F(x)$.

(where $H(x)$ is the Heaviside step function), ρ, τ_0 and $\tilde{\tau}_0 = \rho^{-\frac{1}{3}}\tau_0$ are all zero for $x < 0$, and for $x > 0$ behave as shown in figure 2. The pressure peak is downstream of the peak wall indentation, and the wall shear peak is still further downstream. It can be seen that both p and τ_0 decay algebraically as $x \to +\infty$, not exponentially like $f: p \propto x^{-\frac{2}{3}}$, $\tau_0 \propto x^{-\frac{1}{3}}$. For future reference we note the solution when $f, \tilde{f}$ themselves vary algebraically:

$$f = \phi x^{\alpha} H(x), \quad \tilde{f} = \tilde{\phi} x^{\alpha} H(x), \tag{3.5}$$

with $\alpha > 0$. Then

$$p = \frac{3\,\mathrm{Ai}'(0)\,(\phi + \beta\tilde{\phi})}{1 + \beta\rho^{-\frac{5}{3}}} \frac{\Gamma(1+\alpha)}{\Gamma(\frac{4}{3}+\alpha)} x^{\alpha+\frac{1}{3}} H(x), \tag{3.6}$$

$$\tau_0 = \frac{3\,\mathrm{Ai}(0)\,(\phi + \beta\tilde{\phi})}{1 + \beta\rho^{-\frac{5}{3}}} \frac{\Gamma(1+\alpha)}{\Gamma(\frac{2}{3}+\alpha)} x^{\alpha-\frac{1}{3}} H(x). \tag{3.7}$$

Recalling that $\mathrm{Ai}'(0) < 0$ while $\mathrm{Ai}(0) > 0$, we see that, as expected, the pressure gradient becomes adverse and the wall shear perturbation becomes negative only when the overall cross-sectional area of the channel increases with x, i.e. $-b = \phi + \beta\tilde{\phi} < 0$. The magnitude of p grows with x for all $\alpha > 0$, while the wall shear perturbation grows only if $\alpha > \frac{1}{3}$; it is interesting that the wall shear is independent of x if $\alpha = \frac{1}{3}$.

3.2. *Large-amplitude limit*

This is the limit $h \to \infty$, taken after all the other limits, so that $\epsilon h \ll 1$, for example. In this case most of the wall layer responds in an inviscid manner to the imposed perturbation, relegating viscous effects to an even thinner layer at the wall, of thickness $\epsilon h^{-\frac{1}{3}} a_0$. Of course, that viscous layer is a classical boundary layer, in which the pressure gradient, of $O(h^2)$, is imposed from outside, rather than an interactive boundary layer like the primary one, so it will inevitably experience a Goldstein singularity for a sufficiently adverse pressure gradient. Nevertheless the solutions are revealing, because they provide an analytical indication of non-unique solutions to the boundary-layer problems posed in §2.

For inviscid flow, the vorticity in the boundary layers remains uniform, and the solutions are:

$$U = Y+F+A, \quad V = -Y(F'+A'), \quad \tilde{U} = \rho(\tilde{Y}+\tilde{F}-A/\beta), \quad \tilde{V} = -\tilde{Y}\rho(\tilde{F}'-A'/\beta)$$

so the pressure gradient is given by both

$$-P' = (F+A)(F'+A')$$

and

$$-P' = \rho^2(\tilde{F}-A/\beta)(\tilde{F}'-A'/\beta).$$

We deduce, therefore, that

$$(F+A)^2 = \rho^2(\tilde{F}-A/\beta)^2,$$

which has two solutions for A:

$$A_1 = -\frac{F+\rho\tilde{F}}{1-\rho/\beta}, \quad A_2 = -\frac{F-\rho\tilde{F}}{1+\rho/\beta}. \tag{3.8}$$

The corresponding pressure gradient are

$$P_1' = -\frac{1}{2(\beta/\rho-1)^2}\frac{\mathrm{d}}{\mathrm{d}x}(F+\beta\tilde{F})^2, \tag{3.9a}$$

$$P_2' = -\frac{1}{2(\beta/\rho+1)^2}\frac{\mathrm{d}}{\mathrm{d}x}(F+\beta\tilde{F})^2, \tag{3.9b}$$

while the slip velocities on $Y = 0$ and $\tilde{Y} = 0$, U_s and $\tilde{U}_s$ respectively, are given by

$$U_{s1} = -\tilde{U}_{s1} = -\frac{F+\beta\tilde{F}}{\beta/\rho-1}, \tag{3.10a}$$

$$U_{s2} = +\tilde{U}_{s2} = +\frac{F+\beta\tilde{F}}{\beta/\rho+1}; \tag{3.10b}$$

if a slip velocity is positive it can be thought of as corresponding to an attached flow, and if it is negative to a separated flow, although in the latter case there would not be a solution for the viscous sublayer, so the flow would not be realizable. However, the above solutions do suggest the possibility of having either 'symmetric' flows (the second solution), attached on both walls when the cross-sectional area of the annulus is lower than its unperturbed valve ($F+\beta\tilde{F} > 0$), and separated on both walls when it is higher, or 'asymmetric' flows, attached on one wall and separated on the other (the first solution). It is interesting to note that both solutions involve a favourable pressure gradient whenever $F+\beta\tilde{F}$ is increasing in magnitude, whatever its sign. It should also be remarked that the first solution is singular in the planar limit $\rho = \beta = 1$. Probably the only one of these solutions to be physically realizable is the second solution in the case of narrowing area and favourable pressure gradient, $F+\beta\tilde{F}$ positive and increasing.

3.3. *Similarity solutions*

Here we bridge the gap between small- and large-amplitude flows, not by providing numerical solutions to the coupled boundary-layer problems of (2.10–2.11), but by concentrating on a wall shape that permits a similarity solution, so that only ordinary differential equations need to be integrated numerically.

Similarity solutions can be found when, for $x > 0$,

$$F = \phi x^{\frac{1}{3}}, \quad \tilde{F} = \tilde{\phi} x^{\frac{1}{3}}, \tag{3.11}$$

and the corresponding forms for $A(x)$ and $P(x)$ are

$$A = \Phi x^{\frac{1}{3}}, \quad P = \tfrac{3}{2}\Delta x^{\frac{2}{3}}. \tag{3.12}$$

The boundary-layer thicknesses also increase like $x^{\frac{1}{3}}$, and the longitudinal velocities in them do too. Thus in the layer on the inner wall we write

$$U = x^{\frac{1}{3}}g'(\eta), \quad V = \tfrac{1}{3}x^{-\frac{1}{3}}(\eta g' - 2g), \quad \eta = Y/x^{\frac{1}{3}},$$

and equations (2.10) are satisfied if

$$g''' + \tfrac{2}{3}gg'' - \tfrac{1}{3}g'^2 = \Delta, \tag{3.13}$$

where

$$g(0) = g'(0) = 0, \tag{3.14}$$

and

$$g'(\eta) \sim \eta + \phi + \Phi \quad \text{as} \quad \eta \to \infty. \tag{3.15}$$

Similarly on the outer wall we set

$$\tilde{U} = x^{\frac{1}{3}}\tilde{g}'(\tilde{\eta}), \quad \tilde{V} = \tfrac{1}{3}x^{-\frac{1}{3}}(\tilde{\eta}\tilde{g}' - 2\tilde{g}), \quad \tilde{\eta} = \tilde{Y}/x^{\frac{1}{3}},$$

where $\tilde{g}(\tilde{\eta})$ also satisfies equation (3.13) and boundary conditions (3.14), but the outer boundary condition is

$$\tilde{g}'(\tilde{\eta}) \sim \rho(\tilde{\eta} + \tilde{\phi} - \Phi/\beta) \quad \text{as} \quad \tilde{\eta} \to \infty. \tag{3.16}$$

Equation (3.13) is familiar as the Falkner–Skan equation, but the different boundary condition at infinity, and the coupling of the equations for the two boundary layers, introduce a number of novel features to the solution. Note that a positive value of Δ corresponds to a positive value of $\mathrm{d}P/\mathrm{d}x$, and hence to an adverse pressure gradient.

We note first that (3.13) can be rescaled to take one of two standard forms, depending only on the sign of Δ and not on its magnitude. Setting

$$g(\eta) = \chi^{-1}G(z), \quad z = \tfrac{2}{3}\chi^{-1}\eta, \tag{3.17}$$

where

$$\chi = (\tfrac{2}{3})^{\frac{3}{4}}|\Delta|^{-\frac{1}{4}}, \tag{3.18}$$

we obtain

$$G''' + GG'' - \tfrac{1}{2}G'^2 = s, \tag{3.19}$$

where $s = \pm 1$, and the inner boundary conditions (3.14) remain unchanged:

$$G(0) = G'(0) = 0. \tag{3.20a}$$

Thus, if we were to specify the wall shear rate,

$$G''(0) = \theta, \tag{3.20b}$$

say, we could integrate (3.19) forward in z and achieve two unique solutions (one for each sign on the right-hand side). It can be shown (see Appendix A) that this solution either has a singularity at a finite value of z or tends to the following form at infinity:

$$G(z) \sim \tfrac{1}{2}\zeta z^2 + \gamma z + B + o(1), \tag{3.21}$$

where $\zeta \geqslant 0$; moreover the singular solution is not attained when $s = +1$ (adverse pressure gradient) for any θ. Numerical solution shows further that, when $s = -1$ (favourable pressure gradient), the solution tends smoothly to the form (3.21) if θ exceeds a positive critical value, $\theta_s = 1.5700\ldots$. Numerical integration of (3.19), subject to (3.20a, b), can therefore be use to calculate four universal functions, which we can call $\zeta_\pm(\theta)$, $\gamma_\pm(\theta)$, where $\zeta_\pm$ is the value of $G''(\infty)$ and $\gamma_\pm$ the value of $[G'(z) - \zeta_\pm z]_{z\to\infty}$ for $s = \pm 1$; the + functions are defined for all θ and the − functions are defined only for $\theta > \theta_s$ (note that $\zeta_-(\theta_s) = 0$, corresponding to a conventional

Falkner–Skan boundary layer with a uniform velocity at infinity). The functions $\zeta_\pm(\theta)$ and

$$\kappa_\pm(\theta) = \gamma_\pm(\theta)\,\zeta_\pm(\theta)^{-\frac{2}{3}} \tag{3.22}$$

are plotted over a limited range of θ in figures 3 and 4. The range may easily be extended further, but it is perhaps adequate to note the asymptotic forms, also obtained in Appendix A:

$$\zeta_\pm(\theta) \sim \theta \pm \Gamma(\tfrac{1}{3})(\tfrac{2}{9})^{\frac{1}{3}}\theta^{-\frac{1}{3}} + \ldots, \tag{3.23a}$$

$$\kappa_\pm(\theta) \sim \mp\Gamma(\tfrac{2}{3})(\tfrac{4}{3})^{\frac{1}{3}}\theta^{-\frac{4}{3}} + \ldots \tag{3.23b}$$

as $\theta \to +\infty$, and

$$\zeta_+(\theta) \sim 9.17|\theta|\,(\log|\theta|)^2 \quad \kappa_+(\theta) \sim -4.19\log|\theta| \tag{3.24a, b}$$

as $\theta \to -\infty$. (These asymptotic forms for $\theta \to -\infty$ have interesting implications for grossly separated flow, as discussed in Appendix A, § A 3.)

Armed with these universal functions, solution of the original problem is now only a matter of solving transcendental equations. Let θ be the value of $G''(0)$ corresponding to the inner boundary layer (so that $g''(0) = \frac{4}{9}\chi^{-3}\theta$), and let $\tilde{\theta}$ correspond to the outer layer ($\tilde{g}''(0) = \frac{4}{9}\chi^{-3}\tilde{\theta}$). Then the outer boundary conditions (3.15) and (3.16) give

$$\tfrac{4}{9}\chi^{-3}\zeta_\pm(\theta) = 1, \quad \tfrac{2}{3}\chi^{-2}\gamma_\pm(\theta) = \phi + \Phi, \tag{3.25a, b}$$

$$\tfrac{4}{9}\chi^{-3}\zeta_\pm(\tilde{\theta}) = \rho, \quad \tfrac{2}{3}\chi^{-2}\gamma_\pm(\tilde{\theta}) = \rho(\tilde{\phi} - \Phi/\beta). \tag{3.25c, d}$$

Now Δ, and hence χ, is not known *a priori* and nor is Φ, but ϕ and $\tilde{\phi}$ are known. Eliminating χ from (3.25*a*) and (3.25*b*) and using (3.22) gives

$$\phi + \Phi = (\tfrac{3}{2})^{\frac{1}{3}}\kappa_\pm(\theta) \tag{3.26a}$$

and

$$\beta\tilde{\phi} - \Phi = (\tfrac{3}{2})^{\frac{1}{3}}\beta\rho^{-\frac{1}{3}}\kappa_\pm(\tilde{\theta}). \tag{3.26b}$$

Finally, eliminating Φ gives

$$(\tfrac{3}{2})^{\frac{1}{3}}[\kappa_\pm(\theta) + \beta\rho^{-\frac{1}{3}}\kappa_\pm(\tilde{\theta})] = \phi + \beta\tilde{\phi} \equiv -b; \tag{3.27}$$

the quantity b will henceforth be used to represent the magnitude of the pressure gradient. It is worth remarking that, since $\kappa_+ < 0$ and $\kappa_- > 0$ for all θ for which they exist (figures 3, 4) negative values of b correspond to the minus sign, i.e. a favourable pressure gradient, and positive values to the plus sign, i.e. an adverse pressure gradient. This is exactly as expected, since $\phi + \beta\tilde{\phi} \gtrless 0$ corresponds to a reduction/increase in channel cross-sectional area. Note too that (3.25*a* and *c*) can be used to yield

$$\zeta_\pm(\tilde{\theta}) = \rho\zeta_\pm(\theta), \tag{3.28}$$

and, given θ or $\tilde{\theta}$, either of those equations can be used to determine χ and hence $|\Delta|$ from (3.18).

To find θ and $\tilde{\theta}$ requires solving the transcendental equations (3.27) and (3.28). Consider first flows with favourable pressure gradients, corresponding to $s = -1$ in (3.19), the lower sign in $\zeta_\pm$, and $b < 0$. Given $\rho \leqslant 1$ and $\theta > \theta_s$, $\tilde{\theta}$ can be read off from figure 3 using (3.28), the corresponding values of κ can also be read off from figure 3, and the (negative) value of b can be determined from (3.27). The relationship between θ and b is clearly one-to-one, and can be readily inverted; the problem has a unique solution. The graphs of $-b$ and $\tilde{\theta}$ against θ for the case $\rho = 0.8$ ($\beta = 1.922$) are given in figure 5. The $\tilde{\theta}(\theta)$ graph (figure 5*a*) is virtually linear; in fact $\rho(\theta - \theta_s) - (\tilde{\theta} - \theta_s)$ is zero at $\theta = \theta_s$ and remains extremely small, increasing to only about 0.4 when $\theta = 4.0$. In figure 5(*b*) $-b$ becomes infinite at $\theta = \theta_s$ because $\kappa_-(\theta)$ does; this corresponds

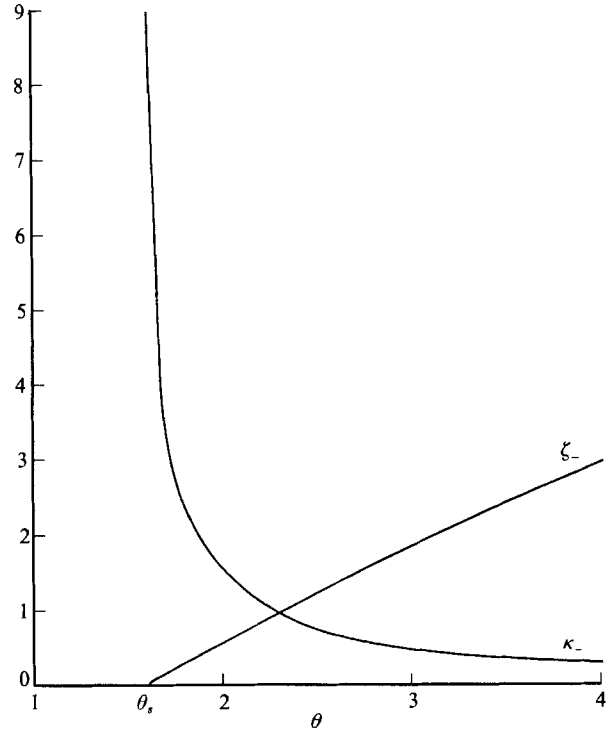

FIGURE 3. Universal functions $\zeta_-(\theta)$, $\kappa_-(\theta)$ for $s = -1$ (favourable pressure gradient).

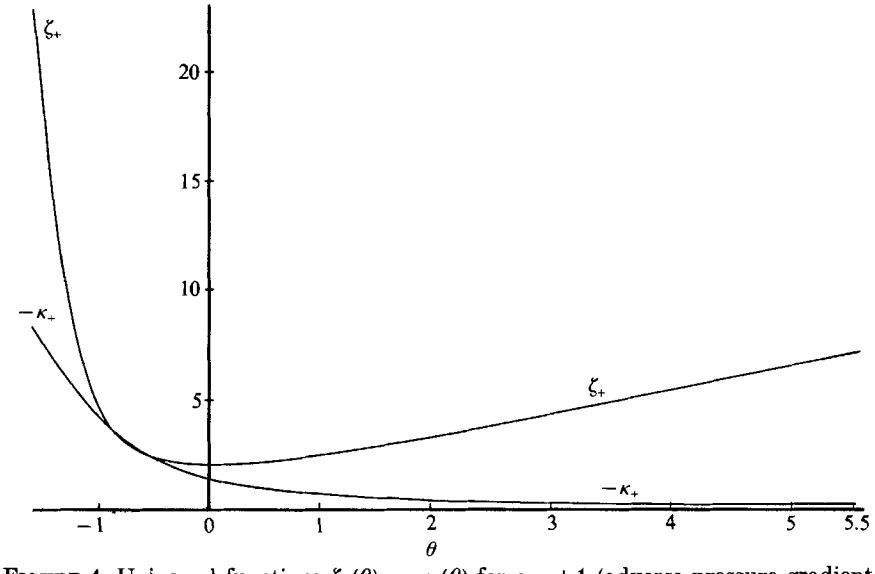

FIGURE 4. Universal functions $\zeta_+(\theta)$, $-\kappa_+(\theta)$ for $s = +1$ (adverse pressure gradient).

to the large-amplitude solution of §3.2. As $\theta \to \infty$, the asymptotic expansions (3.23) can be used with (3.27) to show that

$$\theta^{-\frac{4}{3}} = \frac{2^{-\frac{1}{3}}}{\Gamma(\frac{2}{3})} \frac{\phi + \beta\tilde{\phi}}{1 + \beta\rho^{-\frac{5}{3}}},$$

and together with (3.25a), (3.18) and (3.12) this gives precisely (3.6) for the pressure

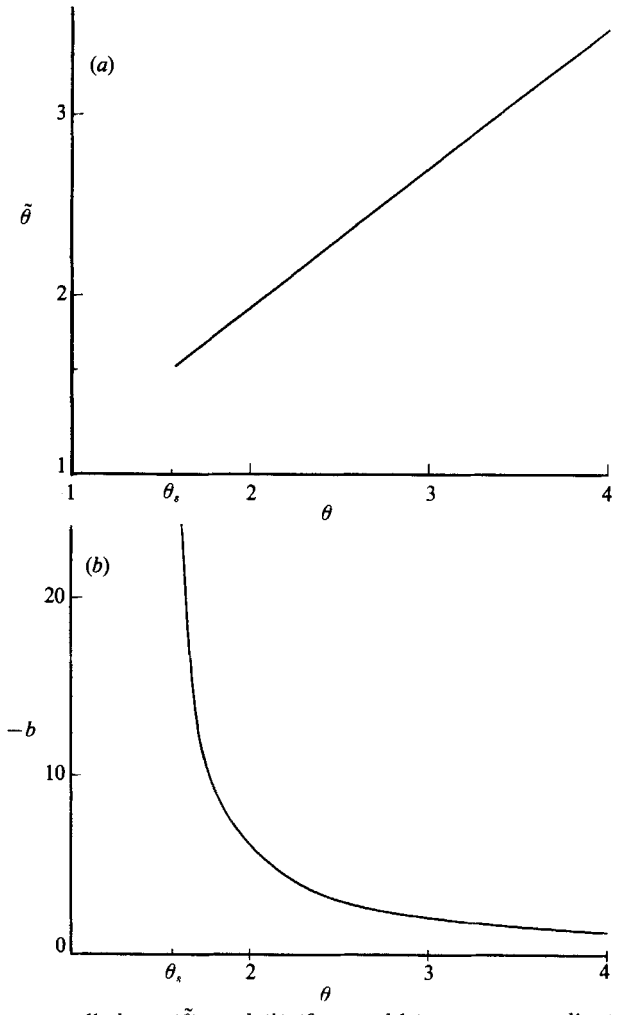

FIGURE 5. (*a*) Outer wall shear ($\tilde{\theta}$), and (*b*) (favourable) pressure gradient ($-b$) as functions of inner wall shear (θ), for $s = -1$, $\rho = 0.8$.

distribution (since $\mathrm{Ai}'(0) = -3^{-\frac{1}{3}}/\Gamma(\frac{1}{3})$). In other words the (unique) solution for a favourable pressure gradient as $\theta \to \infty$ is the same as the small-amplitude solution calculated in §3.1, as expected. (Note that $\rho\theta - \tilde{\theta}$ tends to zero as $\theta \to \infty$, from (3.23*a*) and (3.28), so $\rho(\theta - \theta_s) - (\tilde{\theta} - \theta_s)$ will tend to 0.31.)

Second, we consider flows with an adverse pressure gradient ($s = +1$) and positive b, for which $\zeta_+(\theta)$ and $-\kappa_+(\theta)$ are plotted in figure 4. The curve of $\zeta_+(\theta)$ has a single minimum at $\theta = 0$, with $\zeta_+(0) = \zeta_0 \approx 2.014$ and increases as $|\theta|$ increases (further computation indicates monotonic behaviour between the ends of figure 4 and the asymptotic zones of (3.23) and (3.24)). Thus, for a given θ there are either no corresponding values of $\tilde{\theta}$, if $\zeta_+(\theta) < \rho^{-1}\zeta_0$ (from (3.28)), or there are two such values, one positive and one negative. Therefore there are two (or no) corresponding values of b. A given value of $\zeta_+(\theta)$, and hence a given pair of values of $\tilde{\theta}$, corresponds to a different value of $|\theta|$ according as θ is positive or negative. (It should be remembered that a negative value of θ or $\tilde{\theta}$ means negative shear at the corresponding wall and hence (in that sense) separated flow.) Thus four pairs of graphs like those of figure 5 must be drawn for each value of ρ. Figure 6 has the four graphs of $\tilde{\theta}(\theta)$ for $\rho = 0.8$;

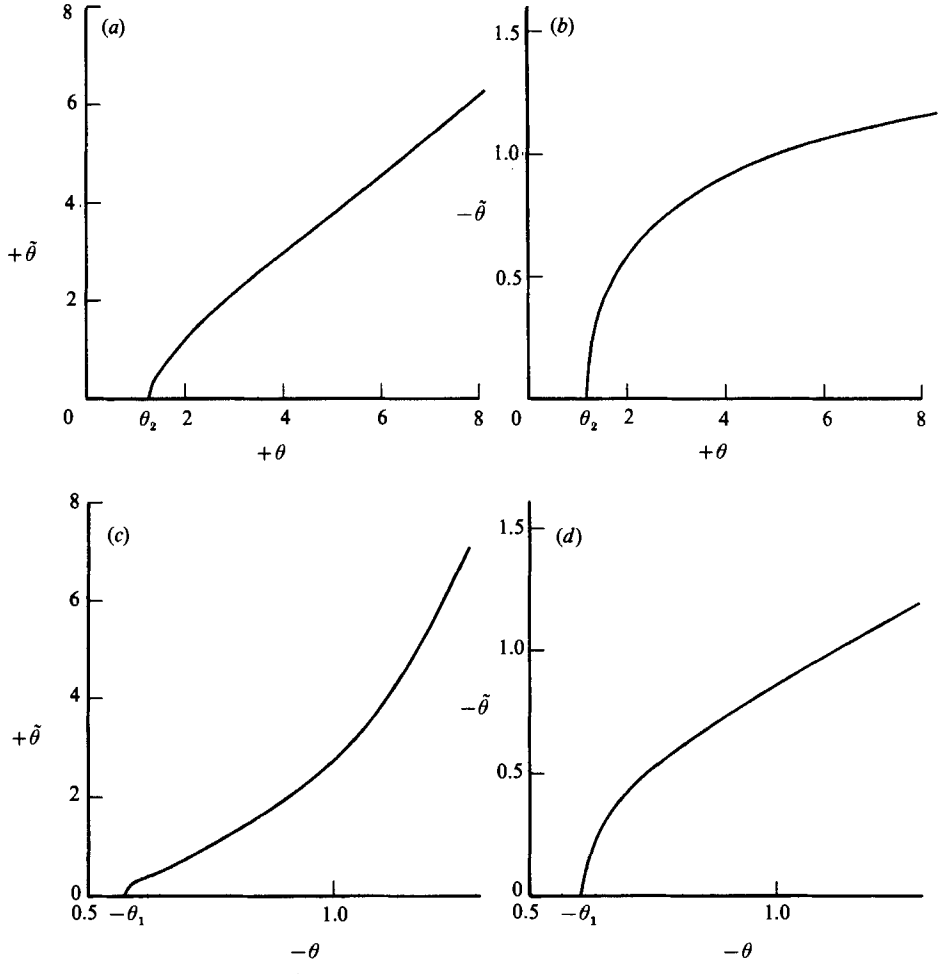

FIGURE 6. Outer wall shear ($\tilde{\theta}$) as a function of inner wall shear (θ) for adverse pressure gradient, $s = +1$, $\rho = 0.8$: (*a*) $\tilde{\theta} > 0$, $\theta > 0$; (*b*) $\tilde{\theta} < 0$, $\theta > 0$; (*c*) $\tilde{\theta} > 0$, $\theta < 0$; (*d*) $\tilde{\theta} < 0$, $\theta < 0$. Note that the scales are different according to the signs of θ, $\tilde{\theta}$.

note that there are no solutions for $\theta_1 < \theta < \theta_2$, where $\theta_1 = -0.58$ and $\theta_2 = 1.09$ (to two decimal places), for $\theta_{1,2}$ are the values of θ at which $\zeta_+(\theta) = \rho^{-1}\zeta_0$ and hence at which $\tilde{\theta} = 0$.

Figure 7 contains in one diagram the four corresponding plots of $b(\theta)$, the four branches of the figure being labelled with the same letters as the four parts of figure 6: (*a*) corresponds to $\theta > 0$, $\tilde{\theta} > 0$; (*b*) to $\theta > 0$, $\tilde{\theta} < 0$; (*c*) to $\theta < 0$, $\tilde{\theta} > 0$; and (*d*) to $\theta < 0$, $\tilde{\theta} < 0$. The two dots are the points of transition between one branch and another, with $\theta = \theta_1$ and θ_2 respectively. It is particularly interesting that b has a minimum value (say b_c, ≈ 5.05), for a negative value of θ that is different from θ_1 (say θ_c, ≈ -0.77).

We are now in a position to determine what flows are possible in a given geometry when the pressure gradient is adverse ($b > 0$). If b is sufficiently small only one flow is possible, represented by branch (*a*), for which both θ and $\tilde{\theta}$ are positive, i.e. the flow on both walls is attached. In the limit of small b ($\theta \to \infty$) this corresponds to the linear solution of §3.1, as in the case of favourable pressure gradient, As b increases above

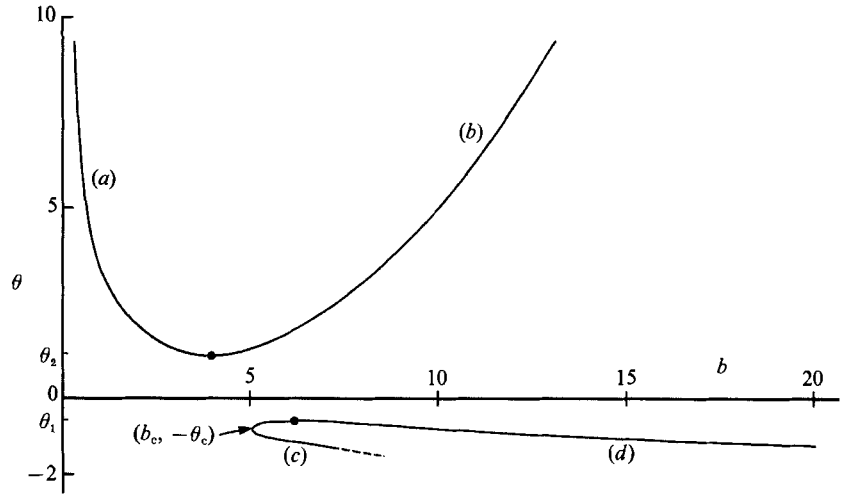

FIGURE 7. θ as a function of b (adverse pressure gradient) for $\rho = 0.8$. Branches (a), (b), and (c), (d), separated by the dots, correspond to the four panels of figure 6.

the value b_2 (≈ 3.96) at which θ is a minimum (θ_2) there is a smooth transition to a still unique state, branch (b), in which $\tilde{\theta} < 0$, and which we can think of as representing a flow which is separated on the outer boundary while still being attached on the inner. However, when b exceeds b_c there is a bifurcation to a state of three possible flows. One is still branch (b), but the other two are, at first, two different examples of flows with $\theta < 0$ and $\tilde{\theta} > 0$ (branch (c)), i.e. separated flow on the inner wall and attached flow on the outer. Only when b exceeds the value b_1 (≈ 6.14), where $\theta = \theta_1$ is a local maximum, does one of these flows experience a smooth transition to one which is separated on both walls, i.e. $\theta < 0$ and $\tilde{\theta} < 0$ (branch (d)). The bifurcation at (b_c, θ_c) is discussed further in §4 below.

The asymptotic expansions (3.23) and (3.24) can be used to derive the form taken by the curves in figures 6 and 7 as $|\theta|$ and $|\tilde{\theta}|$ becomes very large. If both θ and $\tilde{\theta}$ tend to $+\infty$, (branch (a)) then (3.28) with (3.23a) gives $\tilde{\theta} \sim \rho\theta$, and (3.27) with (3.23$b$) gives $b \sim 2^{\frac{1}{3}}\Gamma(\frac{2}{3})(1+\beta\rho^{-\frac{5}{3}})\theta^{-\frac{4}{3}} \to 0$; this limit again recovers the linearized solution. If θ and $\tilde{\theta}$ both tend to $-\infty$ (branch (d)), then (3.28) with (3.24a) again give $\tilde{\theta} \sim \rho\theta$; in this case (3.24$b$) gives $b \sim (\frac{3}{2})^{\frac{1}{3}} 4.19\,(1+\beta\rho^{-\frac{1}{3}})\,(\log|\theta|)$ which tends to infinity. If θ or $\tilde{\theta}$ have opposite signs (branch (b) or (c)), then the positive one will have a much larger magnitude than the negative one, as can be seen from any one of figure 4, figure 6 or the asymptotic expansions, and the negative one will make the dominant contribution to b, which will tend to infinity logarithmically, as on branch (d) of figure 7, but more slowly in either case.

4. Bifurcation diagrams

Figure 7 can be thought of as a bifurcation diagram for the system being investigated, but it does not have a conventional shape, indicating that θ is not a suitable state variable to plot against the bifurcation parameter b. Ideally we would use a variable which tended to zero as $b \to 0$. Moreover, bearing in mind Sobey & Drazin's (1986) results, it is desirable also to have a variable which would be zero for a symmetric flow in a symmetric channel. In that case ($\rho = 1$) such a variable is $\theta - \tilde{\theta}$. A more general state variable which takes that form when $\rho = 1$ and also tends to

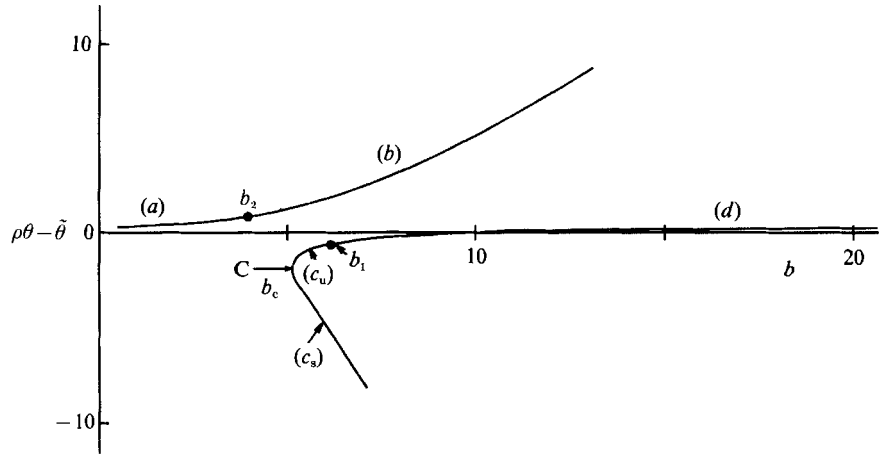

FIGURE 8. Bifurcation diagram of $\rho\theta-\tilde{\theta}$ as a function of b (adverse pressure gradient) for $\rho = 0.8$. Branches (a), (b) and (c), (d), separated by the dots, correspond to the four panels of figure 6. Point C, where $b = b_c$, is a saddle-node bifurcation point; branches (c_u), (d) probably correspond to unstable solutions.

zero when $b \to 0$ is $\rho\theta-\tilde{\theta}$; the second property follows from (3.28) and the asymptotic results (3.23a), as noted at the end of §3. We also saw there that $\rho\theta-\tilde{\theta} \to 0$ as $b \to \infty$ along branch (d). Thus in figure 8 we replot figure 7 with that variable; the dots are again the transition points between the different branches, and the point C is the bifurcation point such that for $b > b_c$ there are three possible solutions. The fact that branch (d) crosses the axis instead of tending to zero probably indicates numerical error in the interpolation scheme used, although much larger values of b would anyway be required for the large-$|\theta|$ asymptotics to be applicable.

Figure 8 is now of familiar form. One would expect that, if b were increased gradually from zero, stable flow on branch (a) would give way to stable flow on branch (b), and that would persist for $b > b_c$. However, different initial conditions could lead to one of the other flows being chosen instead. It is probable that only one of the other possible flows could occur because the other would be unstable. Generically, a bifurcation of the type encountered at C is a saddle-node bifurcation, the saddle branch of which is unstable. Indeed, one can be confident in predicting that the unstable branch is the intermediate one, marked (c_u) and (d) in figure 8, since, again generically, the stability of alternate solution branches also alternates. Moreover, common experience with flow in diffusers indicates that a steady flow that is separated on both walls (branch (d)) is never seen (see §1). The results of the next two paragraphs make the conclusion virtually certain.

The other parameter that can be varied in our system is the geometric parameter ρ, equal to 0.8 in figure 8. It is particularly interesting to see what the results look like for a planar geometry, with $\rho = \beta = 1$, and with an adverse pressure gradient ($-b = \phi+\tilde{\phi} < 0$). The universal functions of figure 4 are of course unchanged, but there are now two values of $\tilde{\theta}$ corresponding to *every* value of $\theta \neq 0$, and $\tilde{\theta} = 0$ when $\theta = 0$. Thus the arguments of §3.4 can be repeated, except that the three critical values, b_1, b_2, b_c on figure 8 coalesce, and there is just one bifurcation point, on the $\theta = 0$ axis. The bifurcation diagram corresponding to figure 8 is given in figure 9. For b small enough, there is one solution on branch (a) with the boundary layer attached on each wall. Because there is no way of distinguishing between the two walls, this

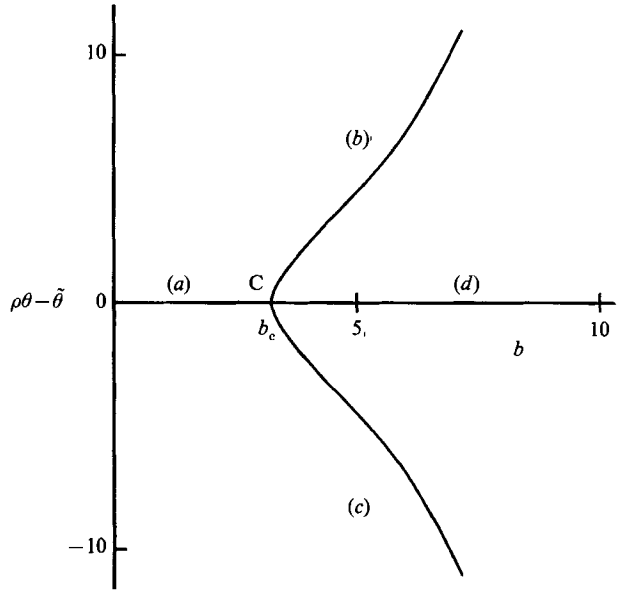

FIGURE 9. As for figure 8, but for a planar channel with $\rho = 1$. The bifurcation at C is a supercritical pitchfork.

flow must be the symmetric one investigated by Smith (1976*a*). However, when $b > b_c$, there are three solutions, only one of which, branch (*d*), can be symmetric (and corresponds to Smith's solution for which symmetry was imposed); this solution represents a flow separated on both walls. The other two solutions, which must be mirror images of each other, are asymmetric ones in which the boundary layer is attached on one wall and separated on the other.

Figure 9 shows a supercritical pitchfork bifurcation, and even without performing a stability analysis we can be certain that branch (*d*) will be unstable, and which of branches (*b*) or (*c*) is chosen in an experiment will depend on chance or small inescapable asymmetries. As soon as ρ is given a value different from 1, however, the symmetry is broken and the diagram takes the form of figure 8. (Note that in this paper ρ is always $\leqslant 1$; a value of $\rho > 1$ merely corresponds to taking θ as the wall shear on the outer, not the inner, wall. If we took $\rho = 1/0.8$, figure 8 would be replaced by its mirror image in the b-axis.) The solutions on branch (c_u) and (*d*) in figure 8 lie on the unstable surface and are presumably unstable. The symmetry breaking can be analysed simply when $1-\rho \ll 1$, as shown in Appendix B.

5. Discussion

It is important to establish both whether the similarity solutions derived above represent real flows, which could be realized with a sufficiently carefully controlled experiment, and whether similar results would be expected for more general wall shapes than those given by (3.11). If the former is true the latter may be expected to follow.

One caveat that ought to be stated first concerning the bifurcation studied in this paper is that it may not be the only one to cause breakdown of symmetric flow in an expanding channel. In practice there could be an instability to a three-dimensional or oscillatory disturbance at a lower Reynolds number than that at which, for a given

adverse pressure gradient, the present non-uniqueness sets in, and the present theory can say nothing about that. The following discussion is made on the assumption that such additional bifurcations are not the first to occur.

The main problem with the wall shapes (3.11) is the fact that their slopes (e.g. $\alpha = \frac{1}{3}\phi x^{-\frac{2}{3}}$) become infinite as $x \to 0+$, so that the small-slope condition for validity of the theory ($\alpha \ll R^{-\frac{3}{7}}$) breaks down at $x \sim \phi^{\frac{3}{11}} R^{\frac{9}{11}}$. However, one can in principle construct a channel for which the slope remains small and $f \sim \phi x^{\frac{1}{3}}$ as $x \to \infty$; a suitable example is

$$f = \frac{\phi x^2}{\mu + x^{\frac{5}{3}}} \tag{5.1}$$

for any positive constant μ, whose maximum slope is $0.636\phi\mu^{-\frac{2}{5}}$. We assume for simplicity that the function f can be expanded in inverse powers of $\xi = x^{\frac{1}{3}}$:

$$f = \phi \sum_0^\infty \phi_n \xi^{1-n}, \quad \phi_0 = 1. \tag{5.2}$$

Then we may seek solutions to the boundary-layer problems defined by (2.10) and (2.11), as $x \to \infty$, in the form of similar expansions:

$$\left.\begin{aligned} P &= \tfrac{3}{2}\Delta \sum_0^\infty P_n \xi^{2-n}, \quad A = \Phi \sum_0^\infty A_n \xi^{1-n}, \\ U &= \sum_0^\infty g_n'(\eta)\, \xi^{1-n}, \quad \text{etc.}, \end{aligned}\right\} \tag{5.3}$$

where $P_0 = A_0 = 1$ and $g_0(\eta)$ is the function $g(\eta)$ discussed in §3.3. The successive problems for $n = 1, 2, 3, \ldots$ are linear, the function $g_n(\eta)$ (representing the inner wall solution) being given by the equation

$$g_n''' + \tfrac{2}{3} g_0 g_n'' + \tfrac{1}{3}(n-2)\, g_0' g_n' - \tfrac{1}{3}(n-2)\, g_0'' g_n + (\tfrac{1}{2}n - 1)\, \Delta P_n = \text{R.H.S.}, \tag{5.4a}$$

where the R.H.S. is known in terms of the lower-order g_j ($j < n$), and the boundary conditions

$$g_n(0) = g_n'(0) = 0, \quad g_n''(\infty) = 0; \tag{5.4b}$$

the last of these follows from the fact that matching to the core-flow shear is fully accomplished by the leading-order solution. This in general there is a unique solution for g_n for each P_n and for a given g_0.

Similarly there is a unique solution for $\tilde{g}_n$ (representing the boundary layer on the outer wall) for each P_n and for a given $\tilde{g}_0$ ($\equiv \tilde{g}$). The other outer boundary conditions ($g_n' \to \phi_n + A_n$, $\tilde{g}_n' \to \tilde{\phi}_n + A_n$) serve simply to determine P_n and A_n. However, the non-uniqueness of the leading term (in the case of adverse pressure gradient) is perpetuated throughout the asymptotic expansions.

These expansions appear to be fully determined by the far downstream solution and therefore not to be affected by different conditions upstream. However, as in conventional boundary-layer theory (Libby & Fox 1963; see also Pedley 1972) it is the appearance of eigensolutions to the homogeneous linear problem (defined by (5.4) with P_n = R.H.S. = 0) which renders the downstream expansion indeterminate, even for a particular g_0. One example of such an eigensolution occurs for $n = 3$, when

$$g_n = \eta g_0' - 2g_0$$

satisfies the homogeneous equation and boundary conditions. Moreover this will be the first eigensolution, since g_n'' is single-signed, without oscillations:

$$g_n'' = \eta g_0''' = \pm A\eta \exp\left(-\frac{2}{3}\int_0^\eta g_0(z)\,\mathrm{d}z\right),$$

from (3.13) (Meksyn 1961). The consequence is that the expansions (5.3) cannot usefully be continued beyond the $n = 2$ terms, but the non-uniqueness of the first few terms is not affected.

To obtain the solution for small x one would expect to be able to integrate numerically, marching forward in x and using the small-amplitude solution of §3.1 to start the integration off as $x \to 0+$. In the annular geometry this approach would presumably trace out a solution branch with the flow attached on both walls for small x, but eventually separated on one wall, corresponding to branch (*b*) of figure 8, if the ultimate adverse pressure gradient (represented by b) were big enough. Quite different upstream conditions, corresponding to particular choices for the amplitude of the large-x eigensolutions, would be needed to converge to one of the other solution branches. In the planar geometry, the marching procedure would naturally encounter the bifurcation point, as in figure 9. The integration would then probably break down unless the solutions were explicitly guided to one branch or the other, for example by *assuming* symmetry between the two boundary layers (as in Smith 1976*a*).

One would expect similar findings for expansions of small slope which do not tend to the simple $x^{\frac{1}{3}}$ form. Numerical solution of the boundary-layer equations can be performed, marching in x as usual, but it will in future be necessary to recognize that a bifurcation point will be reached at a finite value of x (related to the rate of arca expansion) and that multiple solution branches will be found thereafter.

Similar conclusions are also to be expected if the wall slope does not remain very small. In particular Smith (1976*b*) showed that if $\alpha = O(R^{-\frac{3}{7}})$, so that $\lambda = R^{\frac{1}{7}}$ and $\epsilon = R^{-\frac{2}{7}}$ (from 2.4), then the flow structure of an inviscid core with viscous layers on the walls is still predicted, but the cross-stream pressure gradient is no longer negligible in the core. In that case (2.7) gives

$$p \sim \epsilon^2\left[P(x) + A''(x)\int_1^r \frac{U_0^2(r)}{r}\,\mathrm{d}r\right],$$

and the consequence for the boundary-layer problems is that the two pressure gradients are now different, with that in the outer layer being related to that in the inner layer by

$$\tilde{P}(x) = P(x) + \sigma A''(x), \tag{5.5}$$

where

$$\sigma = \int_1^\beta \frac{U_0^2(r)}{r}\,\mathrm{d}r.$$

In the case where F and $\tilde{F}$ are given by (3.11), the above similarity solution is still valid at large x because $A'' \propto x^{-\frac{3}{7}}$ compared with $P \propto x^{\frac{2}{7}}$. The presence of the A'' would influence the large-x expansion of (5.3) only at $n = 7$, and by then the eigensolutions would have made the expansion useless anyway.

The principal effect of a wall slope of $O(R^{-\frac{3}{7}})$ or larger is to generate upstream influence, i.e. a disturbance to the oncoming flow in $x < 0$. Smith (1977) showed how an asymmetric perturbation to a planar channel near $x = 0$ would generate a 'free interaction' upstream. This would first be manifest as a linear disturbance,

proportional to e^{kx}, where $k = 5.731$. Then the boundary layer on one wall would tend to become increasingly compressed while that on the other wall would tend towards separation, which would actally occur at $x = -0.49$ (in dimensional terms, a distance $0.49R^{\frac{1}{7}}h_0$ upstream of the wall disturbance, where h_0 is the channel width). There is no inconsistency between this flow structure and non-uniqueness of the downstream flow at an expansion. It just means that, on the one wall where reversed flow occurs stably downstream, separation may actually take place upstream of the start of the disturbance.

In a subsequent paper, Smith (1979) analysed upstream influence and separation in symmetric, constricted channel flow, showing it to occur only $O(\log R)$ upstream of a symmetric disturbance, not $O(R^{\frac{1}{7}})$. The conclusion of this paper is that, in cases where the channel encounters a sufficiently severe *expansion*, such symmetric flow will never occur, and the $O(R^{\frac{1}{7}})$ structure will always be seen experimentally.

We are grateful to Professor P. G. Drazin for his helpful comments on a previous draft of this paper. Much of this work was done while M.S.B. was a research student at the Department of Applied Mathematics and Theoretical Physics at Cambridge, supported by a George Murray Scholarship from the University of Adelaide, and forms part of his Ph.D. thesis (Borgas 1986). The paper was written while T.J.P. was on sabbatical leave in the George W. Woodruff School of Mechanical Engineering at the Georgia Institute of Technology as the guest of Professor R.M. Nerem, to whom he is most grateful for support and hospitality.

Appendix A. Asymptotic analysis of (3.19) and (3.20)

A.1. *Large z*

The large-z solution of (3.19) takes the form

$$G(z) \sim \tfrac{1}{2}\zeta z^2 + \gamma z + B + o(1), \tag{A 1}$$

where B is given in terms of ζ and γ by

$$B\zeta - \tfrac{1}{2}\gamma^2 = s$$

($s = \pm 1$ according to the sign of the pressure gradient), but ζ and γ will depend on the boundary conditions at $z = 0$, in particular the value of θ. Moreover ζ must be positive, otherwise small departures from (A 1) would grow exponentially; to see that, note that the problem can be manipulated to give

$$G''' = s\exp\left[-\int_0^z G(z')\,\mathrm{d}z'\right]. \tag{A 2}$$

Not every solution of (3.19) tends smoothly to the form (A 1), however, because a singular solution exists:

$$G_s(z) = -4(z_s - z)^{-1} \tag{A 3}$$

for arbitrary z_s. Now (A 2) shows that if $s = +1$ (adverse pressure gradient) then $G'''(z) > 0$, so $G(z)$ cannot tend to the form (A 3) for any $z_s > 0$, and will therefore tend smoothly to the form (A 1). On the other hand, if $s = -1$ (favourable pressure gradient) there is the possibility of encountering the singular solution. Numerical integration shows that the solution tends smoothly to (A 1) if $\theta > \theta_s \approx 1.5700\ldots$. When $\theta \to \theta_{s+}$, $\zeta \to 0_+$ so the solution becomes one of the standard Falkner–Skan functions, which provides a check on the numerical integration.

A.2. *Large* $|\theta|$

We seek asymptotic expansions for $\zeta_\pm(\theta)$ and $\kappa_\pm(\theta)$ as $\theta \to \pm\infty$. For large $|\theta|$ we rescale the problems using

$$z = |\theta|^{-\frac{1}{3}} X, \quad G = |\theta|^{\frac{1}{3}} \bar{G}, \quad \bar{\epsilon} = |\theta|^{-\frac{4}{3}} \tag{A 4}$$

so that the equation and boundary conditions for $\bar{G}(X)$ are

$$\bar{G}''' + \bar{G}\bar{G}'' - \tfrac{1}{2}\bar{G}'^2 = s\bar{\epsilon}, \tag{A 5a}$$

$$\bar{G}(0) = \bar{G}'(0) = 0, \quad \bar{G}''(0) = \operatorname{sgn}(\theta); \tag{A 5b}$$

when $\theta \to +\infty$, s can take either value ± 1, but when $\theta \to -\infty$ only the case $s = +1$ is relevant.

When $X = O(1)$, we seek a solution to (A 5) in powers of $\bar{\epsilon}$:

$$\bar{G} = \tfrac{1}{2}\sigma X^2 + \bar{\epsilon}\bar{G}_1 + \ldots, \quad \sigma = \operatorname{sgn}\theta, \text{ and the } O(\bar{\epsilon})\text{-term is} \tag{A 6}$$

$$\bar{G}_1 = s\left\{\sigma[1 - \exp(-\tfrac{1}{6}\sigma X^3) + \tfrac{1}{2}X^2 \int_0^X \exp(-\tfrac{1}{6}\sigma u^3)\,\mathrm{d}u - X\int_0^X \exp(-\tfrac{1}{6}\sigma u^3)\,u\,\mathrm{d}u\right\}. \tag{A 7}$$

When $\theta \to +\infty$, so $\sigma = +1$, $\bar{G}_1$ remains $O(1)$ for all X and the small-$\bar{\epsilon}$ expansion is uniformly valid. As $X \to \infty$,

$$\bar{G}_1 \sim s\left\{X^2 \frac{\Gamma(\frac{1}{3})}{6^{\frac{2}{3}}} - X\frac{2\Gamma(\frac{2}{3})}{6^{\frac{1}{3}}} + \ldots\right\};$$

hence

$$\zeta = \theta\bar{G}''(\infty) \sim \theta + s\frac{2\Gamma(\frac{1}{3})}{6^{\frac{2}{3}}}\theta^{-\frac{1}{3}}$$

and

$$\gamma = \theta^{\frac{2}{3}}[\bar{G}'(X) - \zeta X]_\infty \sim -s\frac{2\Gamma(\frac{2}{3})}{6^{\frac{1}{3}}}\theta^{-\frac{2}{3}},$$

so

$$\kappa = \gamma\zeta^{-\frac{2}{3}} \sim -s\frac{2\Gamma(\frac{2}{3})}{6^{\frac{1}{3}}}\theta^{-\frac{4}{3}}.$$

These are the results given in (3.23).

When θ becomes large and negative ($\sigma = -1$ and $s = +1$), however, $\bar{G}_1$ grows exponentially. As $X \to \infty$, (A 7) gives

$$\bar{G}_1 \sim 2\exp(+\tfrac{1}{6}X^3)[1 + O(X^{-1})], \tag{A 8}$$

so the expansion breaks down when

$$X = X_c \sim (-6\log\bar{\epsilon})^{\frac{1}{3}}[1 + o(1)], \tag{A 9}$$

and then $\bar{G} = O(X_c^2)$. Numerical integration of (3.19) shows that $\bar{G}$ and its derivatives change rapidly in the vicinity of X_c, with $\bar{G}''$ tending to a positive constant as $X - X_c$ becomes large. The following asymptotic expansion reflects this structure.

Suppose that the rapid variation is characterized by a scale δ. Then the governing equation (in the form $\bar{G}^{\mathrm{iv}} + \bar{G}\bar{G}''' = 0$) shows that $\bar{G}$ must scale with δ^{-1} and it therefore follows that we may take $\delta = X_c^{-2}$. Consequently we make the transformation

$$X = X_c + \delta\bar{\eta}, \quad \bar{G} = \delta^{-1}\tilde{G}(\bar{\eta}) \tag{A 10}$$

so that (A 5a) with $s = +1$ becomes (to leading order)

$$\tilde{G}''' + \tilde{G}\tilde{G}'' - \tfrac{1}{2}(\tilde{G}')^2 = 0. \tag{A 11}$$

The boundary condition as $\bar{\eta} \to -\infty$ is that of matching with (A 6), i.e.

$$\tilde{G} \to -\tfrac{1}{2}X_c^2\delta = -\tfrac{1}{2} \quad \text{as} \quad \bar{\eta} \to -\infty; \tag{A 12}$$

as $\bar{\eta} \to +\infty$ we expect

$$\tilde{G} \sim \tfrac{1}{2}\bar{\zeta}\bar{\eta}^2 + \bar{\gamma}\bar{\eta} + O(1) \tag{A 13}$$

for some constants $\bar{\zeta}(>0)$ and $\bar{\gamma}$. Equation (A 11) subject to (A 12) and (A 13) is equivalent to one that was investigated by Stewartson & Williams (1973); from their numerical solution we may deduce that $\bar{\zeta} = 0.1433$ and $\bar{\gamma}$ is arbitrary, depending on the choice of origin for $\bar{\eta}$. If we rewrite (3.21) in terms of $\bar{\eta}$, using (A 4), (A 9) and (A 10), we eventually obtain

$$\zeta = \bar{\zeta}|\theta|\,(8\log|\theta|)^2, \quad \gamma = -\bar{\zeta}|\theta|^{\frac{2}{3}}(8\log|\theta|)^{\frac{7}{3}} \tag{A 14}$$

from which, with the use of (3.22), (3.24) follows. We may note, incidentally, that convergence of the numerical solutions to these asymptotic forms is extremely slow, as shown in table 1 where the computed and asymptotic values of ζ, and their ratio, are listed for values of $-\theta$ up to 10^7.

$-\theta$	ζ (numerical)	(asymptotic)	Ratio
10^4	2.0×10^7	7.8×10^6	2.6
10^5	2.8×10^8	1.2×10^8	2.3
10^6	3.7×10^9	1.8×10^9	2.1
10^7	4.7×10^{10}	2.4×10^{10}	2.0

TABLE 1. Computed and asymptotic values of ζ and their ratio

A.3. *Implications for grossly separated flow*

For illustration, suppose that only one of the annular walls is distorted, say the outer one so $\phi = 0$, $\tilde{\phi} \to -\infty$; suppose too that the flow is separated on the outer wall and not on the inner ($\tilde{\theta} < 0$, $\theta > 0$: solution branch (*b*) on figures 7 and 8). The above asymptotic expansions, together with the original scalings of §3.3, then show that the thin shear layer that separates the reversed from the forward flow region is approximately centred at $\tilde{Y} = \tilde{\eta}_c X^{\frac{1}{3}}$ where

$$\tilde{\eta}_c = (\tfrac{3}{2})^{\frac{1}{3}}8(\tilde{\zeta}/\rho)^{\frac{1}{3}}\log|\tilde{\theta}|$$

(i.e. $X = X_c$ in (A 9)) which is equal to $-\tilde{\phi}$ in this limit. In other words the shear layer occurs where the outer boundary would have been if there had been no distortion of the wall: the flow in the channel continues undisturbed (confirmed by the fact that $\Phi \to 0$ in this limit) and there is a large reversed-flow eddy the other side of the shear layer. The flow in this eddy is slow, as witnessed by the fact that the (constant) wall shear is given by

$$\tilde{g}''(0) = \tfrac{4}{9}\chi^{-3}\tilde{\theta} \approx -(\tfrac{3}{2})^{\frac{8}{3}}\rho\tilde{\zeta}^{-\frac{1}{3}}\tilde{\phi}^{-2}$$

as $\tilde{\phi} \to -\infty$; this should be compared with the very large wall shear in the attached flow in the inner wall, given by

$$g''(0) = \tfrac{4}{9}\chi^{-3}\theta \approx (\tfrac{2}{3})^{\frac{8}{3}}\tilde{\zeta}^{\frac{1}{3}}\tilde{\phi}^2\exp\left[\tfrac{1}{8}(\tfrac{2}{3})^{\frac{1}{3}}\tilde{\zeta}^{-\frac{1}{3}}|\tilde{\phi}|\right].$$

Furthermore, the adverse pressure gradient, $\Delta x^{-\frac{1}{3}}$, is exponentially small in $|\tilde{\phi}|$, and has negligible effect outside the backflow region.

The above is just one of the three solutions available for large, negative $\tilde{\phi}$. The

other two, branches (*c*) and (*d*), may be similarly analysed. An interesting feature of the problem is that if we have begun with an inviscid analysis, we could have postulated an infinite number of solutions in which the upstream flow is displaced and is bounded on both sides by vortex sheets which separate it from slow, reversed-flow eddies. The two limiting cases in which the flow remains attached on one wall or the other would also be included. The presence of a small viscosity, however, restricts the choice of solutions to three, only one of which is doubly separated in this way. This shows that the eddies, although weak, cannot be entirely passive when viscosity is included.

Appendix B. Analysis of the bifurcation point for $1-\rho \ll 1$

The breaking of symmetry can be investigated analytically for small values of $\epsilon = (1-\rho)^{\frac{1}{3}}$. In this case θ and $\tilde{\theta}$ are both small, and we propose the expansions

$$\theta = \epsilon\theta_1 + \epsilon^2\theta_2 + \ldots, \quad \tilde{\theta} = \epsilon\tilde{\theta}_1 + \epsilon^2\tilde{\theta}_2 + \ldots;$$

we shall also use the small $-\theta$ expansions of ζ_+ and κ_+:

$$\zeta_+ = \zeta_0 + \theta\zeta_1 + \theta^2\zeta_2 + \ldots, \quad \kappa_+ = \kappa_0 + \theta\kappa_1 + \theta^2\kappa_2 + \ldots,$$

where $\zeta_0 = 2.014$, $\zeta_1 = 0$ (because $\theta = 0$ is a minimum of $\zeta_+(\theta)$ – see figure 4), $\kappa_0 = -1.374$, etc. A new, scaled pressure-gradient parameter $\bar{b}$ is defined by

$$b = (\tfrac{3}{2})^{\frac{1}{3}}(-2\kappa_0 + \epsilon^2\bar{b} + \ldots). \tag{B 1}$$

Substitution of these expansions into (3.27) and (3.28) yields $\tilde{\theta}_1 = -\theta_1$, and

$$\theta_1^3 - \lambda_1\bar{b}\theta_1 - \lambda_0 = 0, \tag{B 2}$$

where $\lambda_1 = \zeta_2/(\kappa_1\zeta_3 - 2\kappa_2\zeta_2) = 1.491$, $\lambda_0 = \frac{1}{2}\kappa_1\zeta_0/(\kappa_1\zeta_3 - 2\kappa_2\zeta_2) = 2.355$.

The cubic equation (B 2) is the canonical form for this bifurcation problem; clearly evident is the morphological change from one real solution when $\bar{b}$ is large and negative to three real solutions, $\theta_1 \approx O(\bar{b}^{-1})$, $\pm(\lambda_1\bar{b})^{\frac{1}{2}}$, when $\bar{b}$ is large and positive. In the formal limit $\epsilon \to 0$ but $\epsilon^2\bar{b} = O(1)$ (the planar case) the three solutions become precisely $\theta = 0$, $\pm(\lambda_1\epsilon^2\bar{b})^{\frac{1}{2}}$, as we have found numerically. When $\epsilon \neq 0$, the actual bifurcation point $(\bar{b}_c, \theta_{1c})$ is given (for small ϵ) by

$$\frac{\mathrm{d}\bar{b}}{\mathrm{d}\theta_1} = \frac{\lambda_0 + 2\theta_1^3}{\lambda_1\theta_1} = 0,$$

giving $\theta = -(\frac{1}{2}\lambda_0)^{\frac{1}{3}}$, $\bar{b}_c = 3\lambda_1^{-1}(\frac{1}{2}\lambda_0)^{\frac{2}{3}}$.

For $\rho = 0.8$ ($\epsilon = 0.585$) this gives the bifurcation point (b_c, θ_c) as approximately (4.0, -0.6), which is reasonably close to the exact point marked on figure 7.

REFERENCES

BANKS, W. H. H. & DRAZIN, P. G. 1973 Perturbation methods in boundary layer theory. *J. Fluid Mech.* **58**, 763–775.

BANKS, W. H. H., DRAZIN, P. G. & ZATURSKA, M. B. 1988 On perturbation of Jeffery–Hamel flow. *J. Fluid Mech.* **186**, 559–581.

BORGAS, M. S. 1986 Waves, singularities and non-uniqueness in channel and pipe flows. Ph.D. dissertation, Cambridge University.

FRAENKEL, L. E. 1962 Laminar flow in symmetric channels with slightly curved walls. I. On the Jeffery–Hamel solutions for flow between plane walls. *Proc. R. Soc. Lond.* A **267**, 119–138.

FRAENKEL, L. E. 1963 Laminar flow in symmetric channels with slightly curved walls. II. An asymptotic series for the stream function. *Proc. R. Soc. Lond.* A **272**, 406–428.

LIBBY, P. A. & FOX, H. 1963 Some perturbation solutions in laminar boundary layer theory. Part I. The momentum equation. *J. Fluid Mech.* **17**, 433–449.

MEKSYN, D. 1961 *New Methods in Laminar Boundary-Layer Theory.* Pergamon.

PEDLEY, T. J. 1972 Two-dimensional boundary layers in a free stream which oscillates without reversing. *J. Fluid Mech.* **55**, 359–384.

RENEAU, L. R., JOHNSTON, J. P. & KLINE, S. J. 1967 Performance and design of straight, two-dimensional diffusers. *Trans. ASME* D: *J. Basic Engng* **89**, 141–150.

SMITH, F. T. 1976*a* Flow through constricted or dilated pipes and channels, Part I. *Q. J. Mech. Appl. Maths* **29**, 343–364.

SMITH, F. T. 1976*b* Flow through constricted or dilated pipes and channels, Part II. *Q. J. Mech. Appl. Maths* **29**, 365–376.

SMITH, F. T. 1977 Upstream interactions in channel flows. *J. Fluid Mech.* **79**, 631–655.

SMITH, F. T. 1979 The separating flow through a severely constricted symmetric tube. *J. Fluid Mech.* **90**, 725–754.

SMITH, F. T. 1984 Non-uniqueness in wakes and boundary layers. *Proc. R. Soc. Lond.* A **391**, 1–26.

SOBEY, I. J. 1985 Observation of waves during oscillatory channel flow. *J. Fluid Mech.* **151**, 395–426.

SOBEY, I. J. & DRAZIN, P. G. 1986 Bifurcations of two-dimensional channel flows. *J. Fluid Mech.* **171**, 263–287.

STEWARTSON, K. & WILLIAMS, P. G. 1973 On self-induced separation II. *Mathematika* **20**, 98–108.

WARD-SMITH, A. J. 1980 *Internal Fluid Flow.* Clarendon.